RSC Advances




ROYAL SOCIETY OF CHEMISTRY

www.rsc.org/advances

Journal Name

RSCPublishing

ARTICLE

# Structural and Magnetic Properties of Tetragonal Perovskite $BaFe_{1-x}Bi_xO_{3-\delta}$

Cite this: DOI: 10.1039/xoxxoooooox

Muhammad Asim Farid,[a] Hao Zhang,[a] Xiaohuan Lin,[a] Aimei Yang,[b] Sihai Yang,[c] Guobao Li,*[a] Fuhui Liao,[a] and Jianhua Lin*[a]

Received ooth January 2012,
Accepted ooth January 2012

DOI: 10.1039/xoxxoooooox

www.rsc.org/

A series of $BaFe_{1-x}Bi_xO_{3-\delta}$ ($0.09 \leq x \leq 0.35$) has been synthesized by traditional solid state method. They all crystallize in space group *P4/mmm* (with $a$ = 4.0759(1) Å, $c$ = 4.0782(1) Å for x=0.15) confirmed by the combinational use of powder X-ray, synchrotron, neutron, and electron diffractions. The magnetic susceptibility measurements show that the antiferromagnetic transition for these materials occurs from 64 to 50 K.

## 1. Introduction,

$BaFeO_{3-\delta}$ has been extensively studied for about seventy years,[1-20] which may crystallize in triclinic,[4, 17] monoclinic,[10, 15] orthorhombic,[18] hexagonal,[2, 9, 12, 16] tetragonal,[2] or cubic [13] crystal system depending on the oxygen deficiency and temperature. For example, $BaFeO_{2.80}$ (also noted as $Ba_5Fe_5O_{14}$) crystallizes in orthorhombic crystal system with space group *Cmcm*[19] ( $a$ = 5.7615(8), $b$ = 9.9792(14), and $c$ = 24.347(3) Å at room temperature) with the primary structure being trimers of $FeO_6$ octahedra pillared by dimers of corner-sharing $FeO_4$ tetrahedra, and is noted as 10L-$BaFeO_{3-\delta}$. $BaFeO_{2.91}$ crystallizes in space group $P6_3/mmc$ (a=5.6743(1), $c$ = 13.9298(3) Å at 300 K), [20] and is noted as 6H-$BaFeO_{3-\delta}$. However, due to large ionic radius of Ba it is not easy to synthesize cubic $BaFeO_3$ perovskite phase (noted as C-$BaFeO_3$). Recently, Hayashi et al.[21] reported the low temperature oxidation route to synthesize C-$BaFeO_3$ from $BaFeO_{2.5}$ phase in bulk polycrystalline form. C-$BaFeO_3$ is an antiferromagnet with a spiral spin structure of the A type ($q$//a) that shows a field-induced transition to ferromagnetism at approximately 0.3 T at 5 K (0.2 T at 77 K). In addition cubic $BaFeO_2F$ is antiferromagnetic with $Fe^{3+}$ configuration.[22] It should be very interesting to know what will happen for the perovskite compound $ABO_3$ with both $Fe^{4+}$ and $Fe^{3+}$ at the B site. It is found by us that the perovskite structure can be easily obtained by doping Bi in the Fe site of $BaFeO_{3-\delta}$ with conventional solid state method. A series of solid solution with composition $BaFe_{1-x}Bi_xO_{3-\delta}$ ($0.09 \leq x \leq 0.35$) has been synthesized. With the combinational use of X-ray, neutron, synchrotron, selected area electron diffraction data, and the Mössbauer, Raman/IR spectra, it is found that $BaFe_{1-x}Bi_xO_{3-\delta}$ is the perovskite compound crystallized in the space group *P4/mmm* with both $Fe^{4+}$ and $Fe^{3+}$ at the B site. Magnetic measurements indicate that they are antiferromagnetic ordered below 64 to 50 K. The corresponding details are presented below.

## 2. Experimental

The series of $BaFe_{1-x}Bi_xO_{3-\delta}$ (x = 0.09, 0.12, 0.15, 0.18, 0.21, 0.24, 0.27, 0.30, and 0.35, noted as BFB9, BFB12,…, BFB30, and BFB35) has been synthesized from stoichiometric amounts of reagents $BaCO_3$ (A.R.), $Fe_2O_3$ (A.R.), and $Bi_2O_3$ (A.R.). The weighed reagents were mixed and homogenized by about thirty minute grinding for total 10 g of mixtures with an agate mortar and a pestle. The mixtures were sintered at 840 °C for 12 hours. The sintered mass was again crushed and pulverized to obtain the fine powder. Subsequently, the fine powders were pressed into cylindrical pellets to undertake four 12 hours heat treatments at 880 °C followed by a furnace cooling every time with intermediate grinding and then pressing into pellets. All the treatments were done in air.

Powder X-ray diffraction (PXRD) data were collected on a PANalytical Empyrean diffractometer with Cu $K_{\alpha 1}$ radiation ($\lambda$ = 1.540598 Å) at 50 kV and 40 mA. High resolution synchrotron powder diffraction data were collected on Beamline I11 at Diamond Light Source by using multi-analyzing-crystal detectors (MACs)[23] using an average wavelength of 0.82665 Å, with data points collected every 0.001 º2θ and scan speed of 0.01 º/s. Neutron powder diffraction (NPD) data were collected on the instrument Echidna at the OPAL reactor (Lucas Heights, Australia) in Australian Nuclear Science and Technology Organisation (ANSTO) at $\lambda$ = 2.43950 Å. Sample was placed in 9 mm diameter vanadium can and data collected over 4 hours per sample. The diffraction data were analyzed using GSAS software.[24-25] Selected area electron diffractions (SAED) were carried out on JEM2100F with an accelerating voltage of 200 KV. Raman spectra recorded on a Jobin-Yvon HR800 Raman spectrometer (France); FTIR

spectra were recorded on an ECTOR 22 FTIR spectrophotometer in the region of 650-50 $cm^{-1}$ and a Magna-IR 750 FTIR spectrophotometer in the region of 4000-400 $cm^{-1}$. The magnetic properties were investigated with a Quantum design physical property measurement system (PPMS) from 5 K to 300 K.

The $^{57}$Fe Mössbauer spectra were obtained using $^{57}$Co diffused into rhodium as a source of gamma rays at room temperature.[26] Absolute velocity calibration was carried out with a Fe foil (25 pm thick); isomer shifts (IS) are reported with reference to Fe. The spectra were computer-fitted using a general Lorentzian routine, and a nonlinear least-square curve-fitting procedure was employed to obtain the best fit to the experimental data. We used IS and quadrupole splitting (QS) to characterize the species. The X-ray photoelectron spectroscopy (XPS) patterns were acquired with a UK Kratos Axis Ultra spectrometer with Al Kα X-ray source operated at 15 kV, 15 mA. The chamber pressure was less than $5.0 \times 10^{-9}$ Torr. Electron binding energies were calibrated against the C 1s emission at *E*b = 284.8 eV.

## 3. Results and discussion,

### 3.1. Crystallographic Structure of $BaFe_{1-x}Bi_xO_{3-\delta}$ ($0.09 \le x \le 0.35$).

As shown in Fig.1, the powder X-ray diffraction patterns of the series $BaFe_{1-x}Bi_xO_{3-\delta}$ ($0.09 \le x \le 0.35$) are almost the same and similar to that reported for C-$BaFeO_3$[21]. No reflections for the secondary phase are found. Therefore space group *Pm3m* can be chosen as standard for the refinement of diffraction data.

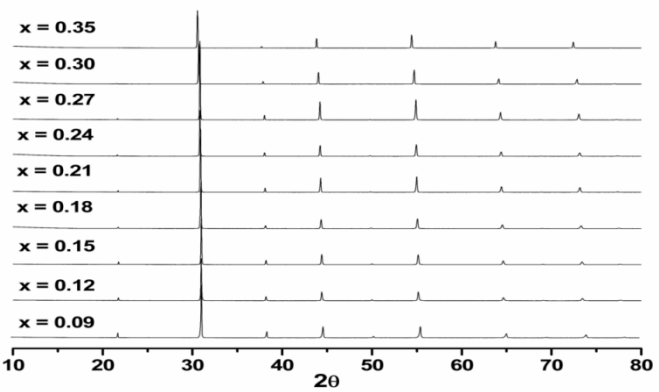


**Fig. 1** Powder X-ray diffraction patterns of the samples in the series $BaFe_{1-x}Bi_xO_{3-\delta}$ ($0.09 \le x \le 0.35$).

The sample BFB15 ($BaFe_{0.85}Bi_{0.15}O_{3-\delta}$) has been chosen as the typical sample. The powder X-ray, synchrotron and neutron diffraction refinement data of BFB15 can be fitted well with space group *Pm3m* as reported for C-$BaFeO_3$.[21] The refinement plots are shown in Figure S1 and the details are listed in Table S1 (supporting information). However room temperature $^{57}$Fe Mössbauer spectra of BFB15 (Figure 2a) shows that it cannot be cubic. Two doublets with an isomer shift of about 0.359(3) and 0.020(4) mm $s^{-1}$ can be derived from the spectra, which indicates the presence of the $Fe^{3+}$ and $Fe^{4+}$ ions with octahedral coordination in non-cubic symmetry. The ratio of $Fe^{3+}$:$Fe^{4+}$ estimated by Mössbauer spectra is 75.4:24.6. At this case, the space group *Pm3m* used for C-$BaFeO_3$[21] could not be used for BFB15.[28] The SAED patterns shown in Fig. 2b for BFB15 indicate that there are no special diffraction conditions. Then the space group *P4/mmm* or *P4mm* can be chosen to describe the structure of BFB15. The mismatch of the Raman peaks and IR peaks for BFB15 shown in Figure 2c indicates that there is a center of symmetry in the structure of BFB15.[27] On careful refinement it is found that the high resolution synchrotron powder diffraction data are also fitted well with space group *P4/mmm*: three peaks are found around 62.26 °(inset Figure 3a), but only one peak is expected by the space group *Pm3m* (supporting information Figure S1d). Therefore, the space group *P4/mmm* is chosed to describe the structure of BFB15 instead of the space group *Pm3m* for C-$BaFeO_3$. As shown in Fig.3b, the powder x-ray diffraction data of BFB15 can be fitted well by Rietveld refinement using the space group *P4/mmm* with the low R factor values listed in Table 1. For further confirmation, the powder neutron diffraction data were also obtained and shown in Fig. 3c. In addition, the neutron diffraction data were also used to refine the occupation of oxygen, which are listed in Table 1 for BFB15.

Therefore, it is acceptable to use *P4/mmm* to describe the structure of BFB15, which is reasonable to be suggested to describe the structure of BFBn. Acceptable fittings between the experimental data and the proposed model are obtained with Rp<4.10%, Rwp<6.6% for all of the solid solutions (see Supporting Information for details). As shown in Fig.4, the obtained volume of the unit cell increases linearly with the increase of the value of x in $BaFe_{1-x}Bi_xO_{3-\delta}$ due to that the radius of $Bi^{3+}$ or $Bi^{5+}$ is larger than that of $Fe^{3+}$ or $Fe^{4+}$, which agrees well with Vigard's law.[29]

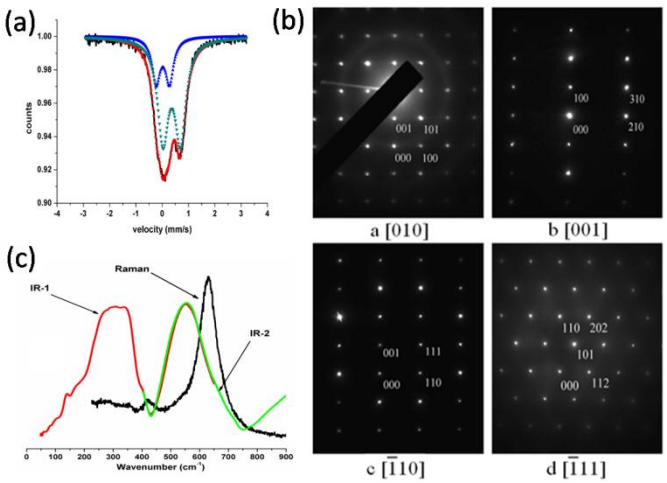


**Fig. 2** $^{57}$Fe Mössbauer spectra at room temperature (a), SAED pattern (b), Raman and IR spectra (c) of BFB15 ($BaFe_{0.85}Bi_{0.15}O_{3-\delta}$).

**Table 1** Rietveld Refinement Details of BFB15 ($BaFe_{0.85}Bi_{0.15}O_{3-\delta}$) in space group *P4/mmm*.

| Lattice parameters | | $a$ = 4.0759(1) Å, $c$ = 4.0782(1) Å | |
|---|---|---|---|
| Atom | (x,y,z) | Occupancy | $U_{iso}$ |
| Ba1 | 0.0000, 0.0000, 0.0000 | 1.00 | 0.0036(3) |
| Fe1 | 0.5000, 0.5000, 0.5000 | 0.85(1) | 0.0072(3) |
| Bi1 | 0.5000, 0.5000, 0.5000 | 0.15(1) | 0.0072(3) |
| O1 | 0.5000, 0.5000, 0.0000 | 0.98(1) | 0.0037(3) |
| O2 | 0.5000, 0.0000, 0.5000 | 0.93(1) | 0.0060(3)u |
| R factor[a] | $R_{wp}^{x}$ = 0.038, $R_{p}^{x}$ = 0.026; $R_{wp}^{s}$ = 0.063, $R_{p}^{s}$ = 0.050; $R_{wp}^{n}$ = 0.064, $R_{p}^{n}$ = 0.044 | | |

[a] $R_{wp}^{x}$, $R_{p}^{x}$ are the R factor of the whole patterns and the peaks only for X-ray diffraction data, respectively; $R_{wp}^{s}$, $R_{p}^{s}$ are the R factor of the whole patterns and the peaks only for synchrotron diffraction data, respectively; $R_{wp}^{n}$, $R_{p}^{n}$ are the R factor of the whole patterns and the peaks only for neutron diffraction data, respectively.

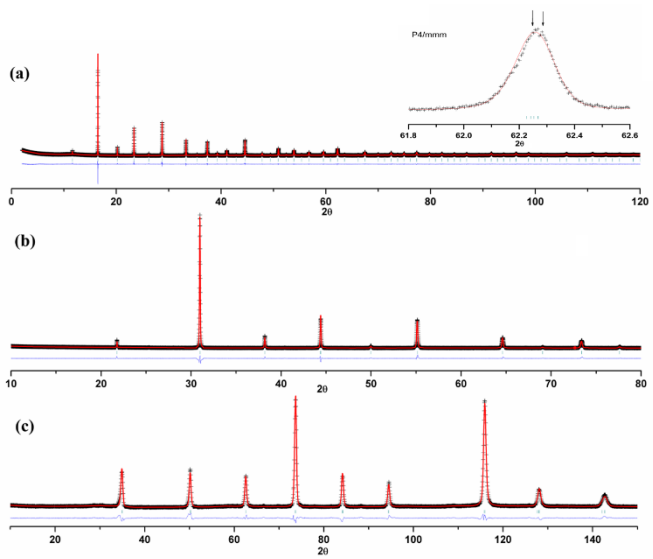


**Fig. 3** Rietveld plots of powder X-ray (a), Synchrotron (b) and neutron (c) powder diffraction pattern diffraction pattern of BFB15 ($BaFe_{0.85}Bi_{0.15}O_{3-\delta}$). The symbol + represents the observed value, solid line represents the calculated value; the marks below the diffraction patterns are the calculated reflection positions, and the difference curve is shown at the bottom of the Figure.

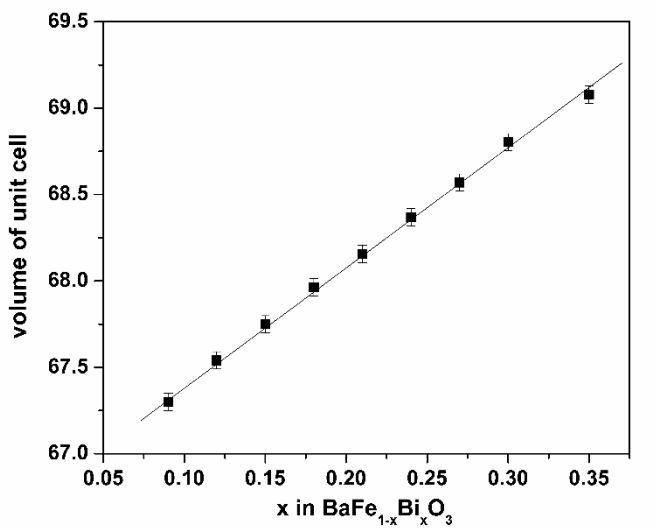


**Fig. 4** volume of the unit cell of $BaFe_{1-x}Bi_xO_{3-\delta}$ ($0.09 \leq x \leq 0.35$) series

### 3.2. XPS Analysis

In order to have a full estimate of the chemical state of Bi and Fe in the series of $BaFe_{1-x}Bi_xO_{3-\delta}$, XPS analysis has been performed. Figure 5 shows the Gaussian fitting of the peaks for Fe $2p_{3/2}$ and Bi $4f_{7/2}$ of BFB15 and BFB24. The Fe $2p_{3/2}$ peaks split into two components as shown in Fig.5a and 5b. The higher energy 710.54 (for BFB15) and 710.92(for BFB24) eV accounts for $Fe^{4+}$ and lower energy 709.84 (for BFB15) and 709.76 (for BFB24) eV belongs to $Fe^{3+}$.[30] The satellite peaks near 718 eV for both of the samples are characteristic of $Fe^{3+}$ ions.[31] In Figure 5c and 5d, the doublet binding energies of Bi $4f_{7/2}$ are due to two valences. The higher binding energy peak around 158.6 eV is characteristic peak for $Bi^{5+}$ while the second peak at lower binding energy is characteristic of $Bi^{3+}$ as described in literature.[32]

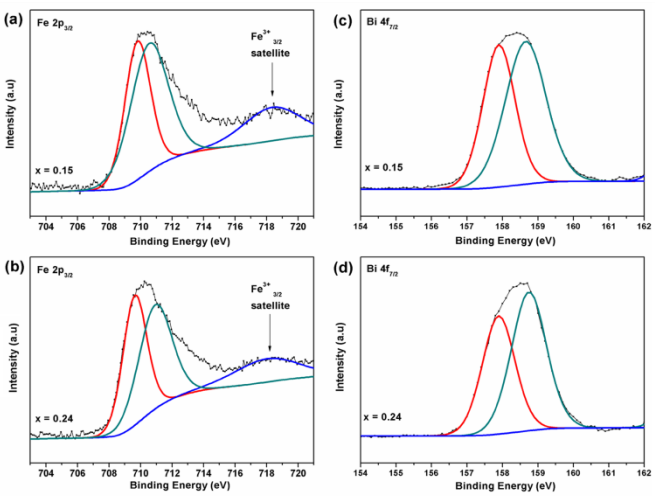


**Fig. 5** XPS spectra of Fe $2p_{3/2}$ (a, b) and Bi $4f_{7/2}$ (c, d) for BFB15 ($BaFe_{0.85}Bi_{0.15}O_{3-\delta}$) and BFB24 ($BaFe_{0.76}Bi_{0.24}O_{3-\delta}$)

A comparison of Fe $2p_{3/2}$ and Bi $4f_{7/2}$ core levels for the whole series $BaFe_{1-x}Bi_xO_{3-\delta}$ ($0.09 \le x \le 0.35$) are shown in Figure 6. It is found that the Fe $2p_{3/2}$ peaks significantly shift towards the lower binding energy direction with the increase in concentration of Bismuth in solid solutions (Figure 6a). This means the gradual decrease in charge at the Fe site, which leads to a chemical shift to a lower binding energy. Simultaneously the binding energies for Bi $4f_{7/2}$ shift towards higher energy state as shown in Figure 6b. It is due to the gradual relative increase in $Bi^{5+}$ concentration. Therefore, it can be speculated that with the increase of the amount of Bi in the sample, the relative amounts of $Bi^{5+}$ and $Fe^{3+}$ increase, although it is obvious that the present data could not give the clear results for the ratio of $Fe^{3+}$:$Fe^{4+}$ and $Bi^{5+}$:$Bi^{3+}$.

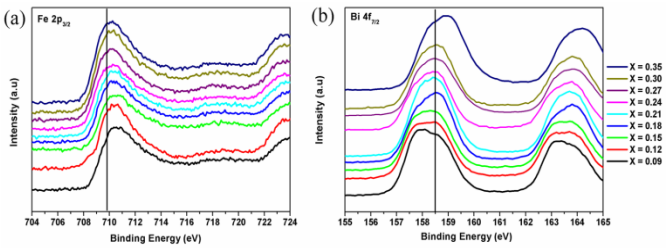


**Fig. 6** XPS spectra of Fe $2p_{3/2}$ (a) and Bi $4f_{7/2}$ (b) for the series $BaFe_{1-x}Bi_xO_{3-\delta}$ ($0.09 \le x \le 0.35$)

### 3.3. Magnetic Properties

The variation of magnetic susceptibility with increasing temperature from 5 K to 300 K following pre-cooling in zero applied field (ZFC) and an applied field (FC) of 100 Oe was measured for all of the samples in the series of $BaFe_{1-x}Bi_xO_{3-\delta}$. The ZFC and FC data overlie over a large temperature range (70-300 K). Typical data for BFB15 and BFB24 are shown in Figure 7 (the data for other samples listed in Supporting I). The susceptibilities from 100 K to 300 K are fitted well by a Curie-Weiss law with the Curie constants and Weiss temperatures (θ) listed in Table 2.

The ratio of $Fe^{3+}$:$Fe^{4+}$ can be estimated from the $C_{obt}$ by supposing that $Fe^{3+}$ and $Fe^{4+}$ in the sample are at high spin state, which is listed in Table 2 and agrees well with the ratio of $Fe^{3+}$:$Fe^{4+}$ obtained by Mössbauer spectra for BFB15. The ratio of $Fe^{3+}$:$Fe^{4+}$ increase with the increase of Bi in the samples also agrees well the observation by XPS. The dominant exchange interactions are antiferromagnetic as θ values are negative. The ZFC and FC susceptibilities rise and start to diverge near 64 K to 50 K for different samples in the solid solutions. This is typical for the canted antiferromagnetic compounds. These temperatures are Neel temperature, and noted as $T_N$. The decrease in $T_N$ was observed as a function of increase concentration of bismuth in B site as listed in Table 3, which may be the result of the decrease of the ratio of $Fe^{4+}$ in the samples.

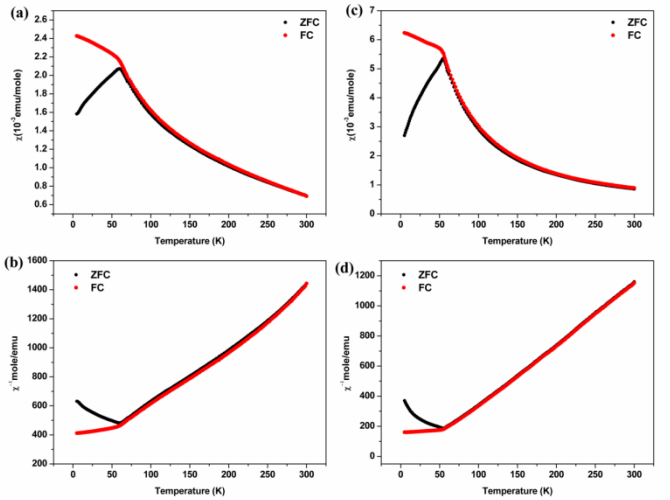


**Fig. 7** Molar magnetic susceptibility χ and inverse molar magnetic susceptibility $\chi^{-1}$ verses temperature for BFB15 ($BaFe_{0.85}Bi_{0.15}O_{3-\delta}$) (a, b) and for BFB24 ($BaFe_{0.76}Bi_{0.24}O_{3-\delta}$) (c, d). Empty and filled symbols show field cooling (FC) and zero-field cooling (ZFC) data, respectively.

**Table 2** $T_N$, θ, $\mu_{eff}$ and Curie Constant of the $BaFe_{1-x}Bi_xO_{3-\delta}$ samples

| x | $T_N$ (K) | θ(K) | Curie Constant | $Fe^{3+}$:$Fe^{4+}$ (%) |
|---|---|---|---|---|
| 0.09 | 64 | -20 | 3.93 | 67.3(3):32.7(3) |
| 0.12 | 62 | -22 | 3.96 | 69.3(3):30.7(3) |
| 0.15 | 60 | -25 | 4.02 | 74.5(3):25.5(3) |
| 0.18 | 58 | -11 | 4.03 | 75.5(3):24.5(3) |
| 0.21 | 57 | -8 | 4.05 | 76.6(3):23.4(3) |
| 0.24 | 56 | -3 | 4.07 | 77.6(3):22.4(3) |
| 0.27 | 54 | -17 | 4.11 | 80.7(3):19.3(3) |
| 0.30 | 53 | -19 | 4.13 | 81.8(3):18.2(3) |
| 0.35 | 50 | -16 | 4.18 | 85.0(3):14.0(3) |

Field dependent magnetic susceptibility has also been measured for $BaFe_{1-x}Bi_xO_{3-\delta}$. Magnetization curves for BFB15 and BFB24 at 5, 55, and 75K are shown in Figure 8. At 75K, the magnetization curves are a linear function of applied field because the samples at this temperature are paramagnetic. It is not surprised that no obvious hysteresis loop is observed at 55K because which is just a little lower than the $T_N$. A little hysteresis is observed at 5 K with the loop displaced from the origin. This is agreed well with the suggestion that the studied samples are canted antiferromagnetic.

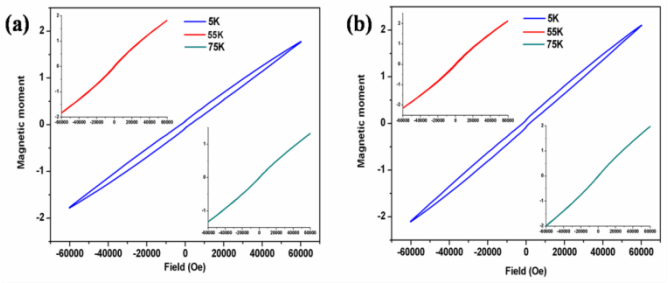


**Fig. 8** M-H curve for BFB15 ($BaFe_{0.85}Bi_{0.15}O_{3-\delta}$) (a) and BFB24 ($BaFe_{0.76}Bi_{0.24}O_{3-\delta}$) (b) at 5K, 55K and 75K.

### 3.4. Neutron diffraction study

Neutron powder diffraction data for BFB15 have been collected at 3 K, 55 K and 300 K to understand of the magnetic properties of $BaFe_{1-x}Bi_xO_{3-\delta}$. These data are shown in Figure 9a. It is found that the main reflections are very similar and can be fitted well with the same structural model used for BFBn at room temperature as shown in Figure 10a. However, with a fine comparison among these neutron diffraction patterns, some little additional satellite peaks are observed in range of 35-40 degree 2θ value for neutron diffraction data at 3 K and 55 K as shown in Figure 9b, which are similar to that of C-$BaFeO_3$[21] at low temperature. These additional reflections are due to incommensurate magnetic ordering of Fe ions with q = (0.195, 0.153, 0.000) and $\mu_{eff}$ = (2.69, 3.95, 0.00)$\mu_B$ at 55K and q = (0.195, 0.150, 0.000) and $\mu_{eff}$ = (3.30, 4.40, 0.00)$\mu_B$ at 3K. The corresponding Rietveld refinement data at 55K are listed in Figure 10c.

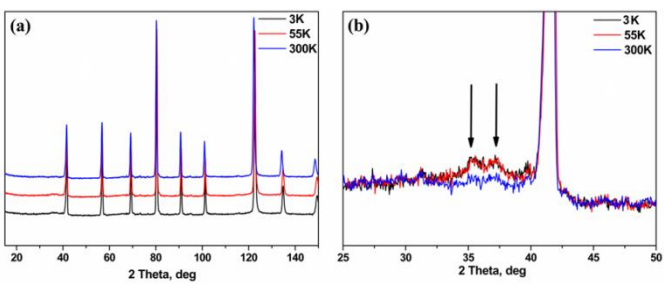


**Fig. 9** Neutron powder diffraction pattern for BFB15 ($BaFe_{0.85}Bi_{0.15}O_3$) at 3 K，55 K and 300 K

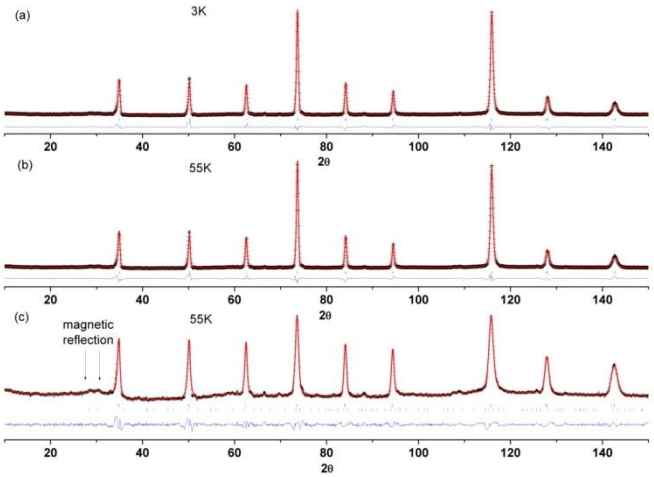


**Fig. 10** Rietveld refinement of the neutron data of BFB15 ($BaFe_{0.85}Bi_{0.15}O_3$) at 3K with nuclear structure (a), at 55K with nuclear structure (b), and at 55K with both nuclear and magnetic structure (c).

## 4. Conclusions

A new series of $BaFe_{1-x}Bi_xO_{3-\delta}$ ($0.09 \leq x \leq 0.35$) solid solutions has been synthesized by solid-state reactions under 880°C calcinations. They all crystallize in tetragonal structure with P4/mmm space group. XPS shows that the ratios of $Fe^{3+}$:$Fe^{4+}$ and $Bi^{5+}$:$Bi^{3+}$ increase with the increase of Bi in the $BaFe_{1-x}Bi_xO_{3-\delta}$ series. Magnetic measurement and neutron diffraction data indicate that $BaFe_{1-x}Bi_xO_{3-\delta}$ is an incommensurate antiferromagnet ($q$≈(0.195, 0.150, 0.000) for BFB15) when the temperature below $T_N$.

## Acknowledgements

This work is supported by a National Key Basic Research Project of China (2010CB833103), the National Natural Science Foundation of China (Grant 21271014). We thank Dr. M. Avdeev for assistance in collecting the neutron power diffraction data at the OPAL facility. We are grateful to Diamond Light Source for access to Beamlines I11.

## Notes and references

[a]Beijing National Laboratory for Molecular Sciences State Key Laboratory of Rare Earth Materials Chemistry and applications College of Chemistry and Molecular Engineering Peking University, Beijing 100871 (P.R. China)
Fax: (+86) 10-6275-3541
E-mail: liguobao@pku.edu.cn
[b]A College of Materials and Engineering, Institution Guangxi Guilin University of Technology, Guilin 541004, China
[c]School of Chemistry University of Nottingham University Park, Nottingham NG7 2RD, UK

† Footnotes should appear here. These might include comments relevant to but not central to the matter under discussion, limited experimental and spectral data, and crystallographic data.

Electronic Supplementary Information (ESI) available: [details of any supplementary information available should be included here]. See DOI: 10.1039/b000000x/

1 M. Erchak, I. Fankuchen and R. Ward, *Journal of the American Chemical Society*, 1946, **68**, 2085-2093.
2 W. W. Malinofsky and H. Kedesdy, *Journal of the American Chemical Society*, 1954, **76**, 3090-3091.
3 H. J. V. Hook, *The Journal of Physical Chemistry*, 1964, **68**, 3786-3789.
4 S. Mori, *Journal of the American Ceramic Society*, 1966, **49**, 600-605.
5 T. Negas and R. S. Roth, *Journal of Research of the National Bureau of Standards Section a-Physics and Chemistry*, 1969, **A 73**, 425-+.
6 S. Mori, *Journal of the Physical Society of Japan*, 1970, **28**, 44-50.
7 M. Zanne, C. Gleitzer and J. Aubry, *Bulletin De La Societe Chimique De France*, 1970, 36-&.
8 M. Zanne and C. Gleitzer, *Bulletin De La Societe Chimique De France*, 1971, 1567-&.
9 A. Jacobson, *Acta Crystallographica Section B*, 1976, **32**, 1087-1090.
10 J. C. Grenier, A. Wattiaux, M. Pouchard, P. Hagenmuller, M. Parras, M. Vallet, J. Calbet and M. A. Alario-Franco, *Journal of Solid State Chemistry*, 1989, **80**, 6-11.
11 M. Parras, M. Vallet-Regi, J. M. Gonz ález-Calbet and J. C. Grenier, *Journal of Solid State Chemistry*, 1989, **83**, 121-131.
12 M. Parras, M. Valletregi, J. M. Gonzalezcalbet, J. C. Grenier, P. Hagenmuller and J. Rodriguezcarvajal, *Eur. J. Solid State Inorg. Chem.*, 1989, **26**, 299-312.
13 M. Parras, J. M. Gonz ález-Calbet, M. Vallet-Reg ía nd J. C. Grenier, *Solid State Ionics*, 1993, **63–65**, 714-718.
14 J. M. Gonzalez-Calbet, M. Parras, M. Vallet-Regi and J. C. Grenier, *Journal of Solid State Chemistry*, 1990, **86**, 149-159.
15 X. D. Zou, S. Hovm öller, M. Parras, J. M. Gonz ález-Calbet, M. Vallet-Reg ía nd J. C. Grenier, *Acta Crystallographica Section A*, 1993, **49**, 27-35.
16 M. G ómez, amp, x, I. a, G. Lucotti, J. A. de Mor án, P. J. Aymonino, S. Pagola, P. Stephens and R. E. Carbonio, *Journal of Solid State Chemistry*, 2001, **160**, 17-24.
17 S. Mori, *Journal of the American Ceramic Society*, 1965, **48**, 165-165.
18 J. M. Gonza lez-Calbet, M. Parras, M. Vallet-Regi ´and J. C. Grenier, *Journal of Solid State Chemistry*, 1990, **85**, 15-22.
19 J. L. Delattre, A. M. Stacy and T. Siegrist, *Journal of Solid State Chemistry*, 2004, **177**, 928-935.
20 K. Mori, T. Kamiyama, H. Kobayashi, K. Oikawa, T. Otomo and S. Ikeda, *Journal of the Physical Society of Japan*, 2003, **72**, 2024-2028.
21 N. Hayashi, T. Yamamoto, H. Kageyama, M. Nishi, Y. Watanabe, T. Kawakami, Y. Matsushita, A. Fujimori and M. Takano, *Angewandte Chemie International Edition*, 2011, **50**, 12547-12550.
22 F. J. Berry, F. C. Coomer, C. Hancock, Ö. Helgason, E. A. Moore, P. R. Slater, A. J. Wright and M. F. Thomas, *Journal of Solid State Chemistry*, 2011, **184**, 1361-1366.
23 S. P. Thompson, J. E. Parker, J. Potter, T. P. Hill, A. Birt, T. M. Cobb, F. Yuan and C. C. Tang, *Review of Scientific Instruments*, 2009, **80**, 075107-075107-075109.
24 H. Rietveld, *Journal of Applied Crystallography*, 1969, **2**, 65-71.
25 B. Toby, *Journal of Applied Crystallography*, 2001, **34**, 210-213.
26 R. M össbauer, *Z. Physik*, 1958, **151**, 124-143.
27 Y. K. Atanassova, V. N. Popov, G. G. Bogachev, M. N. Iliev, C. Mitros, V. Psycharis and M. Pissas, *Physical Review B*, 1993, **47**, 15201-15207.
28 G. Li, S. Liu, F. Liao, S. Tian, X. Jing, J. Lin, Y. Uesu, K. Kohn, K. Saitoh, M. Terauchi, N. Di and Z. Cheng, *Journal of Solid State Chemistry*, 2004, **177**, 1695-1703.
29 L. Vegard, *Z. Physik*, 1921, **5**, 17-26.
30 T. Matsui, E. Taketani, R. Sato and K. Morii, *Journal of Physics D: Applied Physics*, 2007, **40**, 6066.
31 A. P. Grosvenor, B. A. Kobe, M. C. Biesinger and N. S. McIntyre, *Surface and Interface Analysis*, 2004, **36**, 1564-1574.
32 L. Z. Zhao and J. B. Zhang, *Solid State Communications*, 1994, **90**, 709-712.



 